Development 124, 3673-3682 (1997)
Printed in Great Britain © The Company of Biologists Limited 1997
DEV3713

Targeted disruption of the mouse homologue of the *Drosophila polyhomeotic* gene leads to altered anteroposterior patterning and neural crest defects

Yoshihiro Takihara[1], Daihachiro Tomotsune[1], Manabu Shirai[1], Yuko Katoh-Fukui[2], Kiyomasa Nishii[3], Md. Abdul Motaleb[1], Midori Nomura[1], Reiko Tsuchiya[2], Yoshiaki Fujita[2], Yosaburo Shibata[3], Toru Higashinakagawa[2,*] and Kazunori Shimada[1,†]

[1]Department of Medical Genetics, Research Institute for Microbial Diseases, Osaka University, 3-1 Yamadaoka, Suita, Osaka 565, Japan
[2]Mitsubishi Kasei Institute for Life Sciences, Machida, Tokyo 194, Japan
[3]Department of Anatomy, Faculty of Medicine, Kyushu University, 3-1-1 Maidashi, Fukuoka 812-82, Japan

*Present address: Department of Biology, School of Education, Waseda University, 1-6-1 Nishiwaseda, Tokyo 169, Japan
[†]Author for correspondence (e-mail: shimada@biken.osaka-u.ac.jp)

SUMMARY

The *rae28* gene is a mouse homologue of the *Drosophila polyhomeotic* gene (Nomura, M., Takihara, Y. and Shimada, K. (1994) *Differentiation* 57, 39-50), which is a member of the *Polycomb* group (*Pc*-G) of genes (DeCamillis, M., Cheng, N., Pierre, D. and Brock, H.W. (1992) *Genes Dev.* 6, 223-232). The *Pc*-G genes are required for the correct expression of the *Homeotic complex* genes and segment specification during *Drosophila* embryogenesis and larval development. To study the role of the *rae28* gene in mouse development, we generated *rae28*-deficient mice by gene targeting in embryonic stem cells. The *rae28*$^{-/-}$ homozygous mice exhibited perinatal lethality, posterior skeletal transformations and defects in neural crest-related tissues, including ocular abnormalities, cleft palate, parathyroid and thymic hypoplasia and cardiac anomalies. The anterior boundaries of *Hoxa-3, a-4, a-5, b-3, b-4* and *d-4* expression were shifted rostrally in the paraxial mesoderm of the *rae28*$^{-/-}$ homozygous embryos, and those of *Hoxb-3* and *b-4* expression were also similarly altered in the rhombomeres and/or pharyngeal arches. These altered *Hox* codes were presumed to be correlated with the posterior skeletal transformations and neural crest defects observed in the *rae28*$^{-/-}$ homozygous mice. These results indicate that the *rae28* gene is involved in the regulation of *Hox* gene expression and segment specification during paraxial mesoderm and neural crest development.

Key words: *rae28*, *Polycomb* group, *Hox*, segment specification, paraxial mesoderms, neural crest, mouse

INTRODUCTION

In *Drosophila*, the establishment of the expression patterns of the *Homeotic complex* (*HOM-C*) genes are initiated by the maternal effect genes and segmentation genes, and the *HOM-C* genes are responsible for the specification of segmental identity along the anteroposterior (A-P) axis (Gilbert, 1994). The *trithorax* group (*trx*-G) and *Polycomb* group (*Pc*-G) of genes are known to maintain the spatially restricted expression of the *HOM-C* genes in a positive and negative manner, respectively (Krumlauf, 1994; Paro, 1995; Simon, 1995). The Pc-G proteins form multimeric protein complexes and maintain the long-range repression of the *HOM-C* genes, presumably through alterations in the higher-order chromatin structure (Krumlauf, 1994; Paro, 1995; Simon, 1995).

Although evidence is accumulating that vertebrate *Hox* genes have a role similar to that of the *Drosophila HOM-C* genes (McGinnis and Krumlauf, 1992; Krumlauf, 1994), the molecular mechanism regulating the expression patterns of vertebrate *Hox* genes during development is assumed to be different from that in *Drosophila* (Krumlauf, 1994). Since there is very little information available concerning the molecular mechanism regulating the expression of vertebrate *Hox* genes, vertebrate homologues of the *Drosophila trx*-G and *Pc*-G genes have recently attracted attention.

The following mouse homologues of the *Drosophila Pc*-G genes, given in parentheses, have been identified; the *bmi-1* and *mel-18* (*Posterior sex combs*; *Psc*) – van Lohuizen et al., 1991a,b; Haupt et al., 1991; Brunk et al., 1991; Tagawa et al., 1990; *M33* (*Polycomb*; *Pc*) – Pearce et al., 1992; *rae28*/*mph* (*polyhomeotic*; *ph*) – Nomura et al., 1994; Alkema et al., 1997; *eed* (*extra sex combs*; *esc*) – Schumacher et al., 1996; and *ENX-1* genes (*Enhancer of zeste*; *E*(*z*)) – Hobert et al., 1996.

The primary structures of the proteins encoded by these genes are conserved between *Drosophila* and mouse (Simon, 1995; Schumacher et al., 1996; Hobert et al., 1996). As predicted from the *Drosophila Psc*, *esc* and *Pc* gene mutants (Krumlauf, 1994; Paro, 1995; Simon, 1995), the mouse *bmi-1*, *mel-18*, *eed* and *M33* gene mutants showed that these genes are required for proper A-P patterning during mouse development

(van der Lugt et al., 1994; Akasaka et al., 1996; Schumacher et al., 1996; Coré et al., 1997). Moreover, the mouse *M33* gene was demonstrated to have the ability to substitute for the *Drosophila Pc* gene in transgenic flies (Müller et al., 1995). Thus, these mouse homologues of the *Drosophila Pc*-G genes also show functional conservation. Further analysis of vertebrate homologues of the *Drosophila Pc*-G genes should provide important information for understanding the molecular mechanisms which regulate the expression of the vertebrate *Hox* genes.

The *rae28* gene encodes a protein sharing several characteristic motifs and highly homologous regions with the *Drosophila* ph protein; a single zinc finger, a glutamine-rich region and two highly homologous regions, one consisting of 28 amino acid residues and the other, named an H-2/SPM/SEP domain, consisting of 66 amino acid residues (Nomura et al., 1994; Bornemann et al., 1996; Alkema et al., 1997). The RAE28 protein was recently shown to interact with the Bmi-1 and Mel-18 proteins through these conserved domains and to constitute a multimeric protein complex together with the M33 protein (Alkema et al., 1997).

In the present study, we disrupted the *rae28* gene and observed the effects on mouse development. The *rae28*$^{-/-}$ homozygous mice showed skeletal posterior transformations and multiple developmental defects in the eyes, hard palate, parathyroid glands, thymus, heart and spleen. Interestingly, these defects closely resemble the phenotypes of humans with congenital disorders derived from neural crest defects, such as the CATCH-22 syndrome and related disorders (Wilson et al., 1993). *Hox* gene expression was altered not only in the paraxial mesoderms, but also in the rhombomeres and pharyngeal arches of the *rae28*$^{-/-}$ homozygous embryos. Here, we found that the *rae28* gene has a role in the regulation of *Hox* gene expression and the specification of systemic segmental identity, and we also discuss the possible involvement of the *rae28* gene in these congenital disorders derived from neural crest defects.

MATERIALS AND METHODS

Generation of *rae28*-deficient mice

The mouse *rae28* genomic DNA was cloned from a 129/Sv mouse liver genomic library (Motaleb et al., 1996). A 12 kb *Sal*I-*Kpn*I fragment prepared from R5, one of the *rae28* genomic clones, was subcloned into pBluescript (Stratagene, La Jolla, CA). The promoterless neomycin-resistance (*neo*^{r}) gene (Beck et al., 1982) was inserted in-frame in the *Sal*I site of exon 4, and a 5.3 kb *Sal*I-*Eco*RI fragment was deleted (Motaleb et al., 1996). The D3 embryonic stem (ES) cells were electroporated with 25 μg/ml of the construct linearized with *Sal*I and *Kpn*I, plated at a density of 7×10^6 cells per 15 cm feeder plate and selected with G418 (300 μg/ml) (Episkopou et al., 1993; Takeuchi et al., 1995). After 11-14 days, G418-resistant (G418^r) colonies were screened for homologous recombination by Southern blot analysis with probe A (0.6 kb *Sac*I fragment) and/or probe B (0.5 kb *Kpn*I-*Bgl*I fragment; Fig. 1A; Sambrook et al., 1989; Episkopou et al., 1993; Takeuchi et al., 1995). Probe A was hybridized to *Hin*dIII 6.8 kb wild-type and 5.6 kb recombinant fragments, while probe B was hybridized to *Bsa*I 9.6 kb wild-type and 11.1 kb recombinant fragments. Chimeric mice generated by the injection of positive ES cells into C57BL/6 blastocysts were mated to C57BL/6 females to generate outbred offspring (Hogan, 1994; Episkopou et al., 1993; Takeuchi et al., 1995). Heterozygous mice were backcrossed to C57BL/6 mice for consecutive generations. The genotypes were determined by Southern blot analysis with probe A, as shown in Fig. 1A.

Immunoblot analysis

At 13.5 days post coitum (d.p.c.), embryos were lysed in a buffer containing 100 mM NaCl, 10 mM Tris-HCl (pH 7.6), 1 mM EDTA and 100 μg/ml phenylmethylsulfonyl fluoride. An equal volume of 2× sodium dodecyl sulfate (SDS) sampling buffer was added, and the samples were then clarified by boiling, sonication and centrifugation. The clarified extracts, derived from wild-type, heterozygous and homozygous embryos, were separated by electrophoresis on 10% SDS-polyacrylamide gels. Proteins were transferred to nylon membranes (Millipore, Bedford, MA), immunoblotted with primary antibody raised against a bacterially synthesized RAE28 protein and visualized with horseradish peroxidase-conjugated anti-rabbit IgG (Cappel, Durham, NC) and enhanced chemiluminescent detection reagents (DuPont, Boston, MA) (Ausubel et al., 1987).

Phenotypic analysis

Embryos and newborns were generated from heterozygous intercrosses, and anatomical and histological examinations were performed. The embryos were fixed in 9% formaldehyde, 5% acetic acid and 0.9% picric acid (Bouin's solution; Sigma Chemicals, St. Louis, MO) for at least 24 hours, dehydrated in a graded series of ethanol and embedded in paraffin. Histological sections (2-10 μm) were obtained on a standard paraffin microtome and stained with hematoxylin and eosin (Kaufman, 1992). For skeletal analysis, 17.5 d.p.c. embryos were fixed in Bouin's solution for 24 hours. After removing skin, muscle and viscera, the embryos were dehydrated in 96% ethanol and transferred to acetone for 2 days. Staining was performed in 0.001% alizarin red S and 0.003% alcian blue in 1% acid-alcohol solution for 6 hours at 37°C. Samples were washed in distilled water and cleared for 2 days in 1% KOH, followed by clearing steps in 0.8% KOH and 20% glycerol, in 0.5% KOH and 50% glycerol, and in 0.2% KOH and 80% glycerol for at least 1 week each. Cleared skeletons were stored in 100% glycerol (Kaufman, 1992).

Section in situ hybridization

Wild-type and mutant embryos were obtained and genotyped as described above. Embryos were fixed in phosphate-buffered saline (PBS) containing 4% paraformaldehyde (PFA) and embedded in paraffin. Histological sections (5 μm) were obtained, and mounted on slides coated with 3-aminopropyltriethoxysilane (Sigma). Sections were treated three times with xylene for 3 minutes, and hydrated in an ethanol series (100%, 90%, 70%, 50% ethanol and PBS containing 0.1% Tween-20; PBT). After treatment with 10 μg/ml proteinase K (Sigma) for 10 minutes, sections were fixed again for 10 minutes in PBS containing 4% PFA, treated with 0.2 N HCl, and acetylated in 0.02 N HCl, 1.2% triethanolamine (Wako Pure Chemicals, Osaka, Japan) and 0.02% acetic anhydrate. After being washed in PBT, embryos were soaked in prewarmed prehybridization buffer (50% formamide, 5× SSC, 50 μg/ml yeast total RNA, 1% SDS, 50 μg/ml heparin) for 1 hour at 70°C, and hybridized overnight with a digoxigenin-labeled riboprobe. A riboprobe was synthesized with digoxigenin-UTP and Sp6, T3 or T7 polymerase (Boehringer Mannheim, Mannheim, Germany), using *Hox* genes as templates. After being washed in Solutions I (50% formamide, 5× SSC, 1% SDS), II (50% formamide, 2× SSC) and III (50% formamide, 0.2× SSC) at 70°C and blocking, the sections were incubated overnight at 4°C in the preabsorbed antibody solution. Alkaline phosphatase-conjugated anti-digoxigenin Fab (Boehringer Mannheim) was preabsorbed for 1 hour at 4°C with heat-inactivated mouse embryonic powder (0.6%) and sheep serum (1%). Following further washing in NTMT (100 mM NaCl, 100 mM Tris-HCl [pH 9.5], 50 mM $MgCl_2$, 0.1% Tween, 2 mM levamisol) three times for 10 minutes, an alkaline phosphatase reaction was performed in PVA/NTM solution (12.5% polyvinylalcohol (Aldrich Chemicals, Milwaukee, WI), 100 mM NaCl, 100 mM

Tris-HCl, pH 9.5, 50 mN $MgCl_2$, 2 mM levamisol) containing 300 μg/ml NBT (4-Nitro blue tetrazolium chloride; Boehringer Mannheim) and 150 μg/ml BCIP (5-Bromo-4-chloro-3-indolylphosphate; Boehringer Mannheim). After stopping the reaction, hybridization was observed microscopically (BX50, Olympus, Tokyo, Japan; Wakamatsu and Kondoh, 1990; Sasaki and Hogan, 1993).

RESULTS

Genotyping analysis of mice deficient in the *rae28* gene

The *rae28* gene was disrupted in D3 ES cells (Fig. 1A). Eight of the 80 $G418^r$ clones were found to be targeted for the *rae28* gene by Southern blot analysis with probe A and B (Fig. 1A).

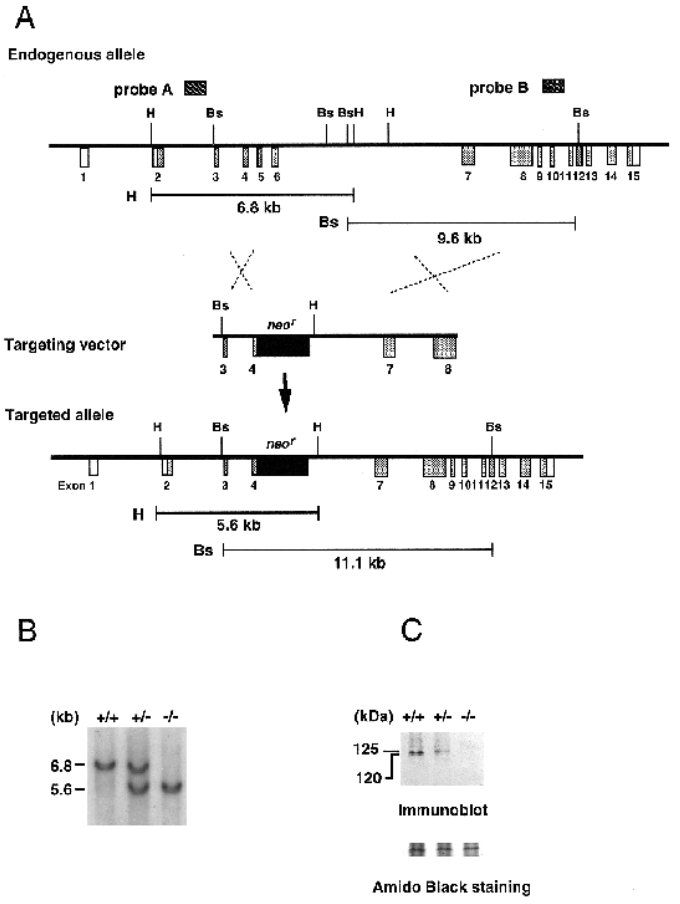

Fig. 1. Targeted disruption of the *rae28* gene by a promoterless neo^r construct. (A) The genomic structure and restriction map of the endogenous *rae28* allele (top), the targeting construct used to disrupt the *rae28* gene in ES cells (middle) and the predicted structure of the targeted allele (bottom). Stippled boxes, coding exons; open boxes, non-coding exons; filled boxes, neo^r gene. The hypothetical crossovers between the endogenous *rae28* allele and the targeting construct are indicated by the crossed dotted lines. The length of diagnostic restriction fragments and the probes used for Southern blot analysis are shown. H, *Hin*dIII; Bs, *Bsa*I. (B) Genotyping of representative offspring by Southern blot analysis with probe A. (C) Immunoblot analysis of offspring from heterozygous intercrosses. The filter was also stained with amido black to show the amount of proteins loaded. +/+, wild-type mice; +/–, heterozygotes; –/–, homozygotes.

These targeted ES clones were injected into C57BL/6 blastocysts to generate chimeric mice. Chimeras transmitting the targeted *rae28* allele to their offspring were obtained with two independent ES cell clones. We obtained offspring from heterozygous intercrosses and determined the genotypes by Southern blot analysis (Fig. 1B). The *rae28* gene expression was not detected in the homozygous embryos by immunoblot analysis (Fig. 1C) and by section in situ hybridization (data not shown). It, however, remains a possibility that an alternative form of *rae28* mRNA was expressed in the homozygous embryos at low levels.

We obtained 369 embryos by Caesarean section at 12.5, 15.5 and 17.5 d.p.c., and examined them for appearance and genotype. Up to 17.5 d.p.c., $rae28^{+/+}$ wild-type, $rae28^{+/-}$ heterozygous and $rae28^{-/-}$ homozygous embryos were present in the expected Mendelian ratios (Table 1). We found that 15 of the 146 newborns were homozygous for the *rae28* mutation (Table 1): 7 of the 15 newborn homozygotes were cyanotic (Fig. 2A) with severe labored breathing, and 2 were already dead. Considering the cannibalized and obviously abnormal $rae28^{-/-}$ homozygotes together, it appears that at least 83% of $rae28^{-/-}$ homozygotes die perinatally. Several homozygous newborn mice were found alive without cyanosis shortly after delivery, but these newborns died of cyanosis within several hours.

Phenotype of the *rae28*-deficient mice

The $rae28^{-/-}$ homozygous mice were smaller than the wild-type and heterozygous mice (Table 2). Abnormalities in the eyes, hard palate, parathyroid glands, thymus, heart, spleen and skeleton of the homozygous embryos and newborn mice were evident (Table 2 and Figs 2-4). Ocular abnormalities ranged from complete absence of the optic cup to hypoplasia (Fig. 2B,C), with or without abnormal rotations of the optic cups. The optic cups of the 12.5 d.p.c. embryos, measured by an image processing method (UTHSCSA *Image Tool* program provided by the University of Texas Health Science Center), were significantly smaller in the homozygotes (Table 2). Interestingly, ocular abnormalities were more prominent on the right side (Table 2). In the frontal histological section of the $rae28^{-/-}$ homozygote shown in Fig. 2C, the right optic cup was completely absent but the hypoplastic optic cup was present on the left. The presence of the retina in the left optic cup was confirmed under high magnification (data not shown). Ten of the 14 $rae28^{-/-}$ homozygous newborns had a bilateral cleft of

Table 1. Genotype of offspring from heterozygous intercrosses

Age	Number of litters	Number of pups	Genotype of the *rae28* gene		
			+/+	+/–	–/–
12.5 d.p.c.	15	121	29	62	30 (2)
15.5 d.p.c.	15	123	30 (2)	63	30 (2)
17.5 d.p.c.	16	125	31	62	31 (4)
NB	19	146	40	91	15 (9)
W5	25	135	40	95	0

Genotypes of offspring were determined by Southern blot analysis. The number of dead mice and/or newborn mice with cyanosis is given in parentheses. d.p.c., days post-coitum; NB, 0-16 hours after birth; W5, 5 weeks old.

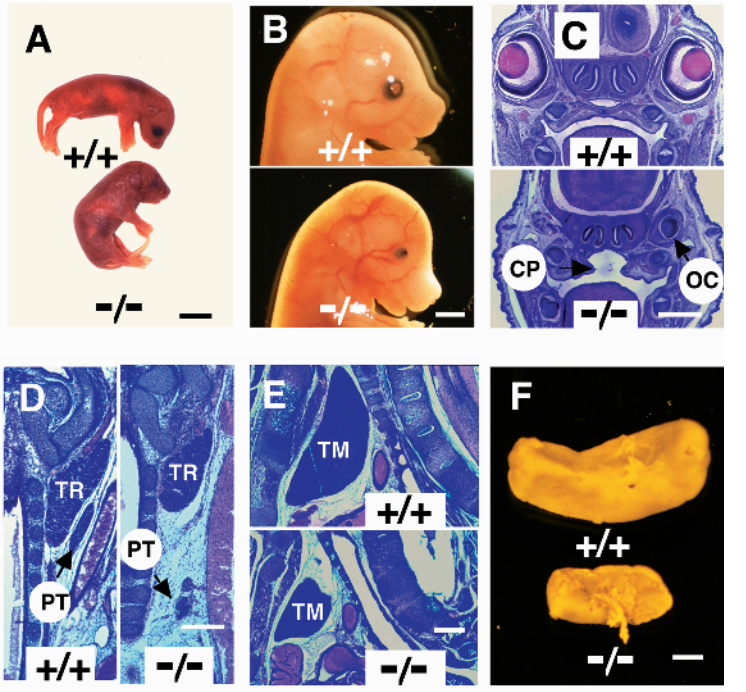

Fig. 2. Phenotype of wild-type (+/+) and homozygous mice (–/–). (A) External appearance of the newborns. Severe cyanosis was observed in homozygotes shortly after birth, but not in wild-type mice. (B) Lateral views of the 15.5 d.p.c. embryos. The eyes were smaller in the homozygous embryos than in the wild-type embryos. (C) Frontal histological sections through the heads of the 17.5 d.p.c. embryos. The right optic cup is completely absent and the left is hypoplastic (OC with an arrow), in the homozygous embryo. Cleft palate is indicated (CP with an arrow). (D,E) Frontal and parasagittal histological sections through cervical and thoracic regions of the 17.5 d.p.c. embryos. TR, thyroid; PT, parathyroid gland; TM, thymus. (F) Fixed spleens isolated from the newborns. Note that the sizes of the thyroid, ectopic parathyroid gland, thymus and spleen are markedly reduced in the homozygotes. Scale bar; A, 5 mm; B,C, 1 mm; D,E,F, 500 μm.

the secondary palate (Table 2 and Fig. 2C). The palate appeared thinner in the other 4 homozygotes than in wild-type mice (data not shown). All homozygotes showed hypoplasia of the parathyroid glands, thymus and spleen, and the positions of the parathyroid glands were markedly altered (Fig. 2D-F). The weights of the thymus and spleen in the homozygotes were almost half of those in the wild-type mice (Table 2). Splenic hypoplasia was present even in the heterozygotes (Table 2).

Serial histological sections of the hearts revealed anomalies in all 12 *rae28*$^{-/-}$ homozygotes, *i.e.*, six 17.5 d.p.c. embryos, one dead newborn, three newborns with cyanosis and two without cyanosis (Table 2 and Fig. 3). Pulmonary stenosis (PS), including infundibular stenosis and pulmonary valve stenosis, was evident in all 12 *rae28*$^{-/-}$ homozygous mice. A ventricular septal defect (VSD) and aortic stenosis (AS) were present in 9 and 6 of the 12 homozygotes, respectively. Four of the 12 homozygotes had tetralogy of Fallot (TOF), one of the most common congenital cardiac anomalies causing cyanosis (Schlant et al., 1994). In the histological section through the right outflow tracts of the homozygous newborn shown in Fig. 3A, stenosis in the right ventricular infundibulum and hypoplasia of the pulmonary trunk were evident. The infundibular chamber (IC) appeared

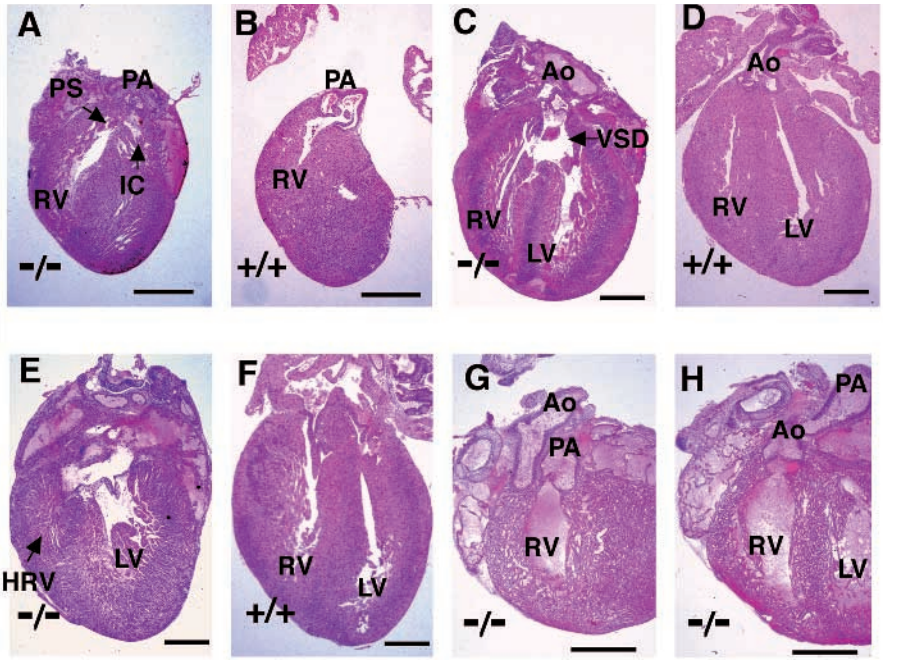

Fig. 3. Cardiac anomalies in homozygous newborns. Serial histological sections of the hearts were observed, and representative hearts from homozygous newborns (–/–; A,C,E,G,H) and wild-type (+/+; B,D,F) are shown. (A-D) Histological sections through the right and left outflow tracts of the homozygous newborns with TOF (A,C) and those of the wild-type (B,D). Stenosis in the right ventricular infundibulum is indicated by PS with an arrow. Hypoplasia of the pulmonary trunk and dilatation of the right ventricle (RV) are noted in A. A large ventricular septal defect is indicated by VSD with an arrow in C. The findings shown in A,C are indicative of TOF. (E,F) Four-chamber histological sections of the hearts. Hypoplasia of the right ventricle is indicated by HRV with an arrow. (G,H) Histological sections through the outflow tracts in a homozygous newborn with DORV. Note that both the aorta and the pulmonary artery originate from the right ventricle. PA, pulmonary artery; Ao, aorta; RV, right ventricle; LV, left ventricle; IC, infundibular chamber; PS, VSD, HRV, DORV, the same abbreviations as in Table 2. Scale bar, 500 μm.

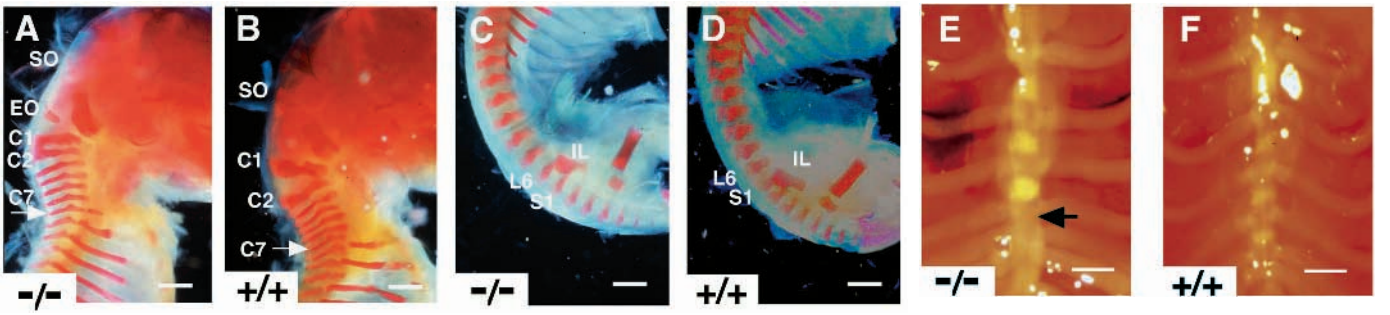

Fig. 4. Skeletal abnormalities in the homozygotes. (A,B) Lateral views of the occipital cervical and thoracic region of skeletons of 17.5 d.p.c. embryos. The wild-type C7 and the homozygous C7 with the ectopic rib are indicated by arrows. (C,D) Lateral views of the lumbar skeletons of the 17.5 d.p.c. embryos. Note that the iliac bone is associated with L6 in the *rae28*$^{-/-}$ homozygous embryos. (E,F) Anterior views of the sternebrae of the newborns. Note loss of the 5th ossification point in the sternebrae of the homozygous newborn, which is indicated by an arrow. –/–, *rae28*$^{-/-}$ homozygous embryos (A,C,E); +/+, wild-type embryos (B,D,F). SO, supraoccipital bone; EO, ectopic ossification between SO and C1; IL, iliac bone; C1, C2, C7, L6, S1, the same abbreviations in Table 2. Scale bar, 1 mm.

between the infundibular stenotic region and pulmonary valve. Enlargement of the right ventricle was confirmed in serial histological sections (data not shown). In addition, the aorta straddled a large ventricular septal defect and originated from both ventricles, as shown in the histological section through the left outflow tract (Fig. 3C). These findings were compatible with TOF, *i.e.*, PS, VSD, biventricular origin of the aorta above VSD and enlargement of the right ventricle (Schlant et

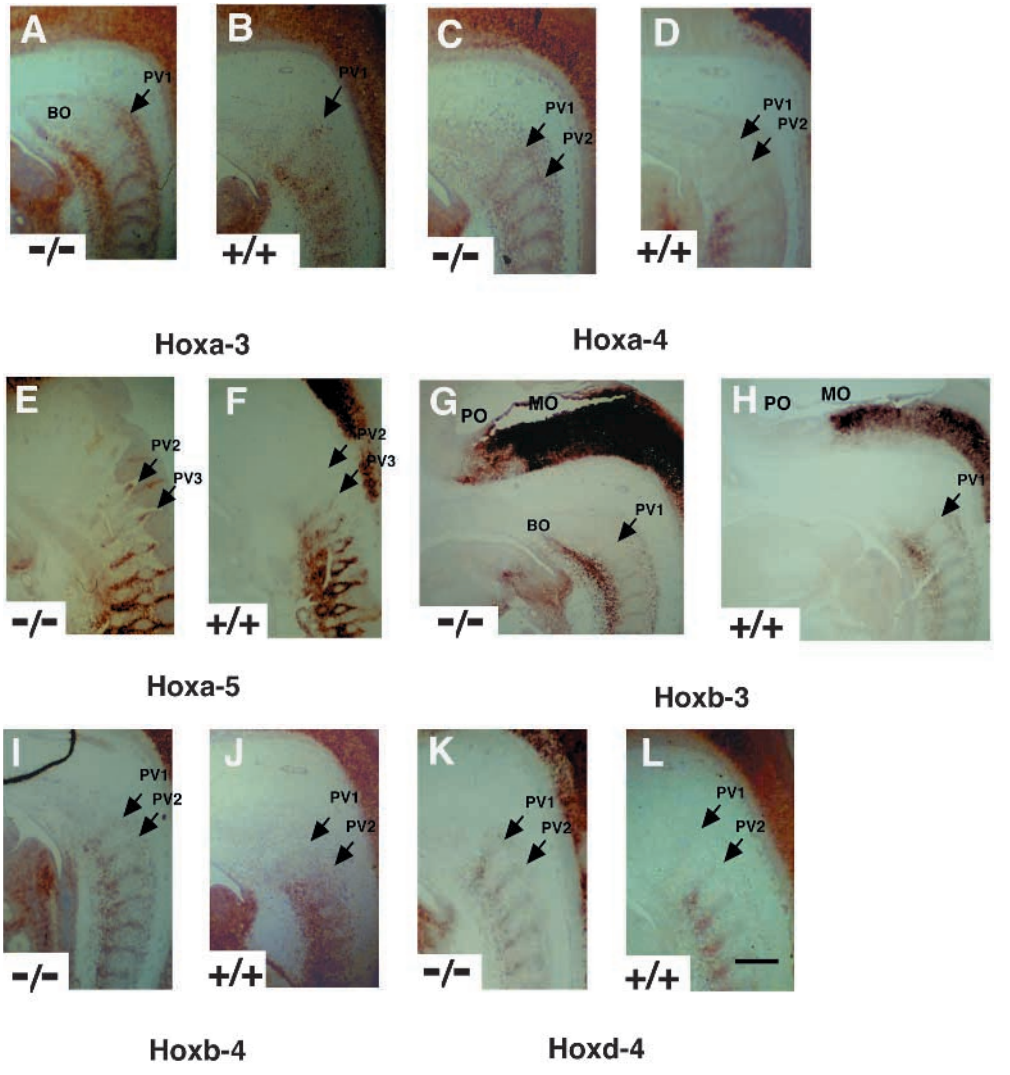

Fig. 5. In situ hybridization with *Hox* probes in the paraxial mesoderm and neural components. Sagittal sections of the 12.5 d.p.c. *rae28*$^{-/-}$ homozygous embryos (–/–; A,C,E,G,I,K) and wild-type embryos (+/+; B,D,F,H,J,L) were hybridized with *Hoxa-3* (A,B), *a-4* (C,D), *a-5* (E,F), *b-3* (G,H), *b-4* (I,J) and *d-4* (K,L) probes. In the *rae28*$^{-/-}$ homozygous embryos, the anterior boundaries of *Hoxa-3* and *b-3* expression, and those of *Hoxa-4*, *b-4* and *d-4* expression spanned the caudal region of the basoccipital anlage and prevertebra 1, respectively. BO, basoccipital anlage; MO, medulla oblongata; PO, pons. PV1, PV2 and PV3 indicate the first, second and third prevertebrae, respectively. The positions of BO, PV1, PV2 and PV3 were confirmed under Nomarski microscopy. Scale bar, 250 μm.

Table 2. Phenotype of offspring from heterozygous intercrosses

	Genotype of the *rae28* gene			*P* value
	+/+	+/–	–/–	(+/+ vs/ –/–)
(a) Mass of newborn mice (g)	(*n*=27)	(*n*=56)	(*n*=15)	
	1.36±0.16	1.37±0.15	1.27±0.14	3.5×10^{-2}
(b) Microphthalmia*	(*n*=24)	(*n*=62)	(*n*=25)	
Left eyes	235±18	234±24	189±35	7.9 ± 10^{-7}
Right eyes	232±19	232±27	156±61	1.2×10^{-6}
(c) Cleft palate†	(*n*=25)	(*n*=56)	(*n*=14)	
	0	0	10	
(d) Parathyroid hypoplasia†	(*n*=4)	(*n*=2)	(*n*=6)	
	0	0	6	
(e) Thymic hypoplasia‡	(*n*=25)	(*n*=51)	(*n*=13)	
	3.04±0.71	3.15±0.67	1.78±0.43	3.9×10^{-8}
(f) Cardiac anomalies†	(*n*=5)	(*n*=3)	(*n*=12)	
PS	0	0	12	
VSD	0	1	9	
AS	0	0	6	
TOF	0	0	4	
DORV	0	0	1	
HRV	0	0	1	
(g) Splenic hypoplasia‡	(*n*=23)	(*n*=50)	(*n*=13)	
	3.30±0.64	2.62±0.58	1.75±0.56	1.4×10^{-8}
(h) Skeletal abnormalities§	(*n*=8)	(*n*=12)	(*n*=7)	
Abnormal supraoccipital bone	0	0	7	
Ectopic occipital ossification	0	0	3	
Fusion of C1 and C2	0	1	5	
C6→T1	0	0	1	
C7→T1	0	0	7	
L6→S1	0	1	4	
Sternal defect	(*n*=26)	(*n*=52)	(*n*=10)	
	0	0	10	

*The index for the size of the optic cup, S, in 12.5 d.p.c. embryos was defined as follows: $S = N/L^2$, where N and L denote the number of pixels in the optic cup counted by the image processing method and the length of the embryos (mm), respectively. The optic cup was smaller on the right side (P=0.013).

†Findings were based on microscopic examinations and serial histological sections of newborns and 17.5 d.p.c. embryos. Abbreviations are as follows: PS, pulmonary stenosis including infundibular stenosis and/or pulmonary valve stenosis; VSD, ventricular septal defect; AS, aortic stenosis; TOF, tetralogy of Fallot; DORV, double-outlet right ventricle; HRV, hypoplasia of the right ventricle.

‡Indices were calculated as follows: the weight (mg) of the isolated thymus or spleen was divided by the weight (g) of the newborns.

§Unilateral and bilateral abnormalities were counted as being positive in the axial skeletal analysis. 'Sternal defect' indicates loss of the 5th ossification point in the sternebrae of the newborns. C1, atlas; C2, axis; C6, 6th cervical vertebra; C7, 7th cervical vertebra; T1, 1st thoracic vertebra; L6, 6th lumbar vertebra; S1, 1st sacral vertebra.

al., 1994). Hypoplasia of the right ventricle (HRV) was observed in one homozygote (Fig. 3E). Serial histological sections of the heart showed that the formation of the entire right ventricle and a tricuspid valve was impaired. Furthermore, we found one homozygous newborn with a double-outlet right ventricle (Schlant et al., 1994). In histological sections through the outflow tracts in this newborn (Fig. 3G,H), both the aorta and the pulmonary artery were found to originate from the right ventricle. Subaortic stenosis in the right outflow tract and atresia in the left outflow tract were present. Both ventricles were severely dilated and the thickness of the myocardium was reduced. No cardiac anomalies were observed in the 5 wild-type and 3 heterozygous mice, except for a minute VSD in one *rae28*$^{+/-}$ heterozygote (Table 2).

We then stained skeletons of the 17.5 d.p.c. embryos and newborns with alizarin red and alcian blue and examined them for morphological changes. All 7 *rae28*$^{-/-}$ homozygotes had skeletal abnormalities, including typical posterior transformations (Table 2 and Fig. 4A,C). Reduced supraoccipital bone and transformation of the seventh cervical vertebra (C7) to the first thoracic vertebra (T1) were obvious in all of the homozygotes. C7 to T1 transformation was evidenced by the presence of ribs in C7 (Fig. 4A). Ectopic ossification between the supraoccipital bone and the atlas (C1), fusion of C1 and the axis (C2), and transformation of the sixth cervical vertebra (C6) to T1 were each present in 1 to 5 of the 7 homozygotes (Table 2). The thickness of the homozygous C1 was reduced and the shape resembled that of C2 (Fig. 4A). All of the newborn homozygotes had sternal defects, including loss of the 5th ossification point in the sternebrae of the newborns (Table 2 and Fig. 4E). Transformation of the sixth lumbar vertebra (L6) to the first sacral vertebra (S1) was present in 4 of the 7 homozygotes. L6

Table 3. Altered anterior expression boundaries of *Hox* genes in mice lacking the *Pc*-G genes

	Genotype			
	rae28$^{-/-}$	*bmi-1*$^{-/-}$	*mel*-18$^{-/-}$	*M33*$^{-/-}$
Hoxa-2	nd (0/2)	nd	nd	nd
Hoxa-3	2/3 (0/4)	nd	nd	+
Hoxa-4	2/2 (0/1)	5/5	nd	nd
Hoxa-5	3/3 (0/2)	2/2	4/4	–
Hoxa-6	nd	nd	nd	–
Hoxa-7	nd	0/2	2/2	nd
Hoxa-9	0/2	nd	nd	nd
Hoxa-10	0/3	nd	nd	nd
Hoxa-11	0/2	nd	nd	nd
Hoxb-1	nd (0/5)	nd	nd	nd
Hoxb-3	*5/5 (5/5)	nd	2/3	nd
Hoxb-4	2/2 (4/4)	nd	4/4	nd
Hoxb-5	0/4	0/2	0/3	nd
Hoxb-6	0/3	3/4	5/6	nd
Hoxb-8	nd	nd	3/3	nd
Hoxc-4	nd	4/4	nd	nd
Hoxc-5	nd	2/2	0/5	–
Hoxc-6	0/5	2/2	1/5	–
Hoxc-8	0/3	4/4	2/3	–
Hoxc-9	nd	2/2	nd	nd
Hoxd-3	0/2 (0/3)	nd	nd	nd
Hoxd-4	3/3 (0/2)	0/2	4/4	–
Hoxd-9	0/2	nd	nd	nd

Summary of ectopic expression of *Hox* genes in mice lacking the *rae28*, *bmi-1* (van der Lugt et al., 1996), *mel-18* (Akasaka et al., 1996) and *M33* genes (Coré et al., 1997). The index is as follows; the number of embryos with ectopic *Hox* gene expression in the paraxial mesoderm/the number of embryos examined. The findings in the rhombomeres are in parentheses. An asterisk indicates that ectopic expression of the *Hox* gene was observed in the paraxial mesoderms and neural components. In the embryos lacking the *M33* gene, the presence and absence of the altered expression boundaries are indicated by plus (+) and minus (–), respectively. nd; not determined.

to S1 transformation was evidenced by the iliac bone associated with L6 instead of S1 (Fig. 4C). Fusion of C1 and C2, and L6 to S1 transformation were also observed in one of the 12 heterozygotes (Table 2).

Ectopic expression of *Hox* genes in the homozygous embryos

Since *Hox* genes are important determinants of segmental identity along the A-P axis (McGinnis and Krumlauf, 1992; Krumlauf, 1994), we examined expression patterns of 15 different *Hox* genes (*Hoxa-3*, *a-4*, *a-5*, *a-9*, *a-10*, *a-11*, *b-3*, *b-4*, *b-5*, *b-6*, *c-6*, *c-8*, *d-3*, *d-4* and *d-9*) in the paraxial mesoderm of 12.5 d.p.c. wild-type and *rae28*$^{-/-}$ homozygous embryos by section in situ hybridization (Table 3). In the wild-type embryos, the anterior boundaries of *Hoxa-3* and *b-3* expression (Fig. 5B,H), and those of *Hoxa-4*, *b-4*, and *d-4* expression spanned PV1 and PV2 (Fig. 5D,J,L), respectively. In the *rae28*$^{-/-}$ homozygous embryos, the anterior boundaries of *Hoxa-3* and *b-3* expression shifted from PV1 to the caudal region of the basoccipital anlage (BO) (Fig. 5A,G), and those of *Hoxa-4*, *b-4*, and *d-4* expression, from PV2 to PV1 (Fig. 5C,I,K). The anterior boundaries of *Hoxa-5* expression were also shifted from PV3 to PV2 in the *rae28*$^{-/-}$ homozygous embryos (Fig. 5E,F). We could not detect ectopic expression of the other *Hox* genes in the paraxial mesoderms (Table 3).

The *rae28*$^{-/-}$ homozygotes showed systemic defects in the neural crest-related tissues (Table. 2). Expression of the four 3′ paralogous *Hox* family members was found in neural crest cells of the rhombomeres and pharyngeal arches (Hunt et al., 1991a-c). Therefore, we further examined the expression patterns of the 3′ *Hox* gene members (*Hoxa-2*, *a-3*, *a-4*, *a-5*, *b-1*, *b-3*, *b-4*, *d-3* and *d-4*) in the rhombomeres and pharyngeal arches of 10.5 d.p.c. wild-type and mutant embryos (Table 3). The rhombomeric segments (R1-R7) and pharyngeal arches (P1-P3) did not appear to be grossly changed histologically in the 10.5 d.p.c. *rae28*$^{-/-}$ homozygous embryos (Fig. 6). In the rhombomeres of the 10.5 d.p.c. *rae28*$^{-/-}$ homozygous embryos, the anterior boundary of *Hoxb-3* expression was shifted from R5 to R4 (Fig. 6B,D) and that of *Hoxb-4* expression, from R7 to R6 (Fig. 6G,H). The anterior boundary of *Hoxb-3* expression in the pharyngeal arches was also shifted from P3 to P2 (Fig. 6B-D). The ectopic expression of the *Hoxb-3* gene in P2 should be correlated with that in R4, because neural crest cells in R4 are known to migrate into P2 (Hunt et al., 1991a-c). In these experiments, R4 and the otic vesicle (OT) were used as landmarks. We also confirmed P2, shown in Fig. 6C, by detecting the anterior boundary of *Hoxa-2* expression in the adjacent section (data not shown) (Hunt et al., 1991a-c).

Furthermore, in 12.5 d.p.c. homozygous embryos, the anterior boundary of *Hoxb-3* expression was shifted from the middle of the medulla oblongata (MO) to the pons (PO) (Fig. 5G,H).

DISCUSSION

In this study, we generated a null mutation of the *rae28* gene by homologous recombination in mouse ES cells. The *rae28*$^{-/-}$ homozygotes showed perinatal lethality and multiple developmental defects. Although some developmental defects appeared in *rae28*$^{-/-}$ homozygotes with incomplete penetrance or expressivity, it is unlikely that this is due to partial inactivation of the *rae28* gene. We have not eliminated the possibility that low levels of an alternatively spliced form of *rae28* mRNA exist in the homozygous mutant embryos, but because we have shown by immunoblot and in situ hybridization analyses that *rae28* expression is not detectable (Fig. 1C and data not shown), we think that if such alternative transcripts exist, they make very little contribution to *rae28* function. Moreover, we do not believe that these partially penetrant phenotypes arose from coincident mutations in the background, since two independent lines gave rise to similar phenotypes. However, we cannot rule out a background effect, because the homozygotes were derived from parents with a hybrid (129/Sv; C57BL/6) background.

The *rae28* mutation affects skeletal A-P patterning and causes the posterior skeletal transformations over the entire A-P axis, *i.e.*, C1 to C2, C7 (C6) to T1 and L6 to S1 transformations (Fig. 4A,C). Similar systemic posterior transformations were observed in mice deficient in other mouse homologues of the *Drosophila Pc*-G genes, such as the *bmi-1*, *mel-18*, *eed* and *M33* genes (van der Lugt et al., 1994; Akasaka et al., 1996; Schumacher et al., 1996; Coré et al., 1997). In the paraxial mesoderms of the *rae28*$^{-/-}$ homozygous embryos, the anterior expression boundaries of the *Hoxa-3*, *a-4*, *a-5*, *b-3*, *b-4* and *d-4* genes were shifted rostrally (Fig. 5A,C,E,G,I,K and

Table 3). These anterior shifts of the *Hox* codes may be correlated with the posterior shift of vertebral identity in the *rae28*$^{-/-}$ homozygotes, because the gain of function by ectopic expression of the *Hox* gene was found to generally result in posterior transformations (McGinnis and Krumlauf, 1992; Krumlauf, 1994; van der Lugt et al., 1994, 1996; Akasaka et al., 1996; Coré et al., 1997).

To our surprise, the *rae28*$^{-/-}$ homozygous mice carried all the phenotypes noted in the human congenital disorder CATCH-22 syndrome (Wilson et al., 1993). The CATCH-22 syndrome encompasses a wide spectrum of clinical manifestations, including cardiac anomalies, abnormal facies with ocular abnormalities, thymic hypoplasia, cleft palate and hypocalcemia (hypoparathyroidism) (Wilson et al., 1993). The CATCH-22 syndrome may include DiGeorge syndrome (McKusick, 1992), vero-cardio-facial syndrome (Shprintzen et al., 1978) and conotruncal anomaly face syndrome (Takao et al., 1980). These syndromes are believed to arise from neural crest defects (Payne et al., 1995; Olson and Srivastava, 1996), because neural crest ablation in the chick rhombomeres produced the similar defects (Bockman and Kirby, 1984; Kirby and Waldo, 1990). The CATCH-22 syndrome is autosomal dominant (Wilson et al., 1993) and is frequently associated with microdeletions within chromosome 22q11 (Wilson et al., 1993; Payne et al., 1995; Olson and Srivastava, 1996). However, most *rae28*$^{+/-}$ heterozygotes do not manifest the overt phenotype, and the *rae28* gene maps to a region syntenic with human chromosome 12p11-p13 (Motaleb et al., 1996). Nevertheless, the remarkable similarity of the phenotypes between the *rae28*$^{-/-}$ homozygotes and the CATCH-22 syndrome may indicate the presence of a defect(s) in a common developmental pathway of neural crest cells.

Expression of the four 3′ paralogous *Hox* family members is found in neural crest cells of the rhombomeres and pharyngeal arches (Hunt et al., 1991a-c), and mutant mice lacking the *Hoxa-1* (Lufkin et al., 1991; Chisaka et al., 1992), *a-2* (Gendron-Maguire et al., 1993; Rijli et al., 1993), *a-3* (Chisaka and Capecchi, 1991; Manley et al., 1995) and *b-1* genes (Studer et al., 1996; Goddard et al., 1996) indicated that these *Hox* genes are involved in neural crest development. The *rae28*$^{-/-}$ homozygous mice share similar defects with the *Hoxa-2*- and *Hoxa-3*-deficient mice, *i.e.*, the *Hoxa-2*-deficient mice showed a bilateral cleft of the secondary palate (Gendron-Maguire et al., 1993; Rijli et al., 1993), and the *Hoxa-3*-deficient mice had defects in the thymus, parathyroid glands and heart (Chisaka and Capecchi, 1991; Manley et al., 1995). It was indicated that these defects in the *Hoxa-2*- and *Hoxa-3*-deficient mice were derived from the neural crest cells in R4 (P2) (Gendron-Maguire et al., 1993; Rijli et al., 1993) and R6+R7 (P3+P4) (Chisaka and Capecchi, 1991; Manley et al., 1995), respectively. R4 and R6 corresponded to the regions where ectopic expression of the *Hoxb-3* and *b-4* genes was found in the *rae28*$^{-/-}$ homozygous embryos (Fig. 6B,C,G). Interestingly, it is known that overexpression of an exogenous *Hox* gene can abrogate the functions of endogenous *Hox* genes to cause phenotypes similar to those of their loss-of-function mutants (Jegalian et al., 1992; Pollock et al., 1992). Therefore, the ectopic expression of the *Hoxb-3* and *b-4* genes in R4 and R6 are presumed to be correlated with the defects in the neural crest-related tissues observed in the *rae28*$^{-/-}$ homozygous mice.

Although multiple *Hox* genes from the three different clusters (*Hoxa-3, a-4, a-5, b-3, b-4* and *d-4*) were found to be affected in the paraxial mesoderms of the *rae28*$^{-/-}$ homozygous embryos (Fig. 5 and Table 3), all of the affected *Hox* genes so far identified were included in the 3 to 5 paralogous families (Table 3). The altered expression of these *Hox* genes

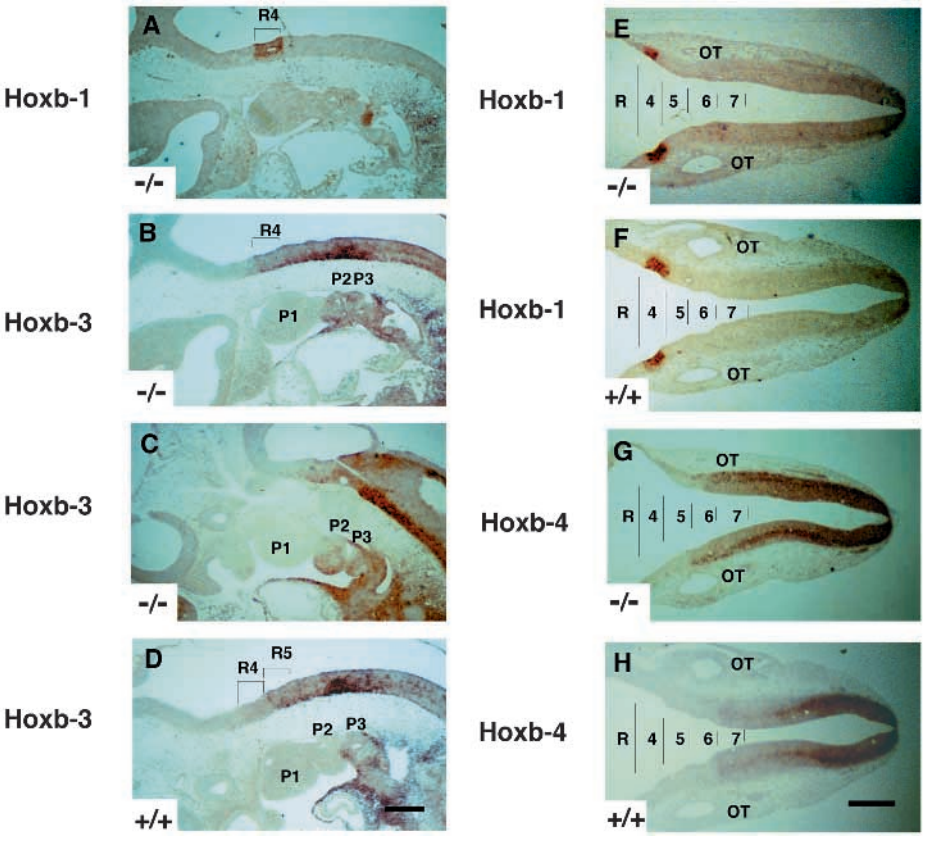

Fig. 6. In situ hybridization with *Hox* probes in the rhombomeres and pharyngeal arches. Sagittal sections (A,B,C,D) and frontal sections (E,F,G,H) through the rhombomeres of the 10.5 d.p.c representative *rae28*$^{-/-}$ homozygous embryos (–/–; A,B,C,E,G) and wild-type embryos (+/+; D,F,H) were hybridized with *Hoxb-1* (A,E,F), *b-3* (B,C,D) and *b-4* (G,H) probes. Note that the anterior boundaries of *Hoxb-3* expression in the rhombomeres and pharyngeal arches of the *rae28*$^{-/-}$ homozygous embryos spanned R4 and P2, respectively (B,C), and that the anterior boundary of *Hoxb-4* expression spanned R6 in the mutant embryos (G). R4, R5, R6 and R7 indicate the fourth, fifth, sixth and seventh rhombomeres, respectively. P1, P2 and P3 indicate the first, second and third pharyngeal arches, respectively. OT, otic vesicle. Scale bar, 250 μm.

was also reported in mice lacking other members of the *Pc*-G genes (Table 3): the *Hoxa-3* gene was affected by the *M33* mutation, the *Hoxa-5* gene was affected by the *bmi-1* and *mel-18* mutations, and the *Hoxa-4*, *b-3*, *b-4* and *d-4* genes were affected by either the *bmi-1* or *mel-18* mutation (van der Lugt et al., 1996; Akasaka et al., 1996; Coré et al., 1997). In contrast, the *Hoxb-6*, *c-6* and *c-8* genes were affected by the *bmi-1* and *mel-18* mutations (van der Lugt et al., 1996; Akasaka et al., 1996), but not by the *rae28* mutation (Table 3). Thus, some of the subset of *Hox* genes affected in the *rae28*$^{-/-}$ homozygous embryos were the same as those affected in mice lacking other members of the *Pc*-G genes. Interestingly, the *Hox* genes affected in the rhombomeres and/or pharyngeal arches of the *rae28*$^{-/-}$ homozygous embryos were restricted to the *Hoxb-3* and *b-4* genes, which are a part of the *Hox* gene subset affected in the paraxial mesoderm (Fig. 6B,C,G and Table 3).

All of these results strongly suggest that the *rae28* gene negatively regulates the expression of a specific subset of *Hox* genes in a tissue-specific manner and is required for proper segmental identity along the A-P axis not only in the paraxial mesoderm but also in the neural crest. Very recently, neural crest defects were also considered to be a factor in compound mutant mice for the *bmi-1* and *mel-18* genes (T. Akasaka, H. Koseki, M. Kanno, M. Taniguchi, N.M.T. van der Lugt and A. Berns, personal communication). Therefore, this is further support for mammalian *Pc*-G genes having a crucial role in neural crest development. Further study of the molecular events underlying the *rae28*$^{-/-}$ phenotype should lead to a better understanding of neural crest development and the related disorders.

We thank Drs H. W. Brock, T., Episkopou, V., Sano, J. Hara, T. Mano, K. Y.-Takihara, T. Takeuchi, T. Takagi and M. E. Gottesman, for their helpful discussions and advice, M. Miyazaki and T. Sakaura for technical support, Dr G. Gaitanaris for providing the *neo*^{r} gene, Dr T. W. Mak for providing the D3 embryonic stem cell line, and Drs D. Duboule, P. Gruss, R. Krumlauf, O. Chisaka, and H. Kondoh for providing *Hox* probes and M. Ohara for helpful comments. We are also grateful for the generous use of Genome information research center. This work was supported by a Grant-in-Aid for Scientific Research from the Ministry of Education, Science, Sports and Culture of Japan, Grants-in-Aid from the Uehara Memorial Foundation, and the Yamanouchi Foundation for Research on Metabolic Disorders.

REFERENCES

Akasaka, T., Kanno, M., Balling, R., Mieza, M.A., Taniguchi, M. and Koseki, H. (1996). A role for *mel-18*, a polycomb group-related vertebrate gene, during the anteroposterior specification of the axial skeleton. *Development* **122**, 1513-1522.

Alkema, M. J., Bronk, M., Verhoeven, E., Otte, A., van't Veer, L. J., Berns, A. and van Lohuizen, M. (1997). Identification of Bmi1-interacting proteins as constituents of a multimeric mammalian Polycomb complex. *Genes Dev*. **11**, 226-240.

Ausubel, F. M., Brent, R., Kingston, R. E., Moore, D. D., Seidman, J. G., Smith, J. A. and Struhl, K. eds. (1987). *Current Protocols in Molecular Biology*, Section 10. 8. Greene Publishing Associates and Wiley-Interscience, New York.

Beck, E., Ludwig, G., Auerswald, E. A., Reiss, B. and Schaller, H. (1982). Nucleotide sequence and exact localization of the neomycin phosphotransferase gene from transposon Tn*5*. *Gene* **19**, 327-336.

Bockman, D. E. and Kirby, M. L. (1984). Dependence of thymus development on derivatives of the neural crest. *Science* **223**, 498-500.

Bornemann, D., Miller, E. and Simon, J. (1996). The *Drosophila Polycomb* group gene *Sex comb on midleg* (*Scm*) encodes a zinc finger protein with similarity to polyhomeotic protein. *Development* **122**, 1621-1630.

Brunk, B. P., Martin, E. C. and Adler, P. N. (1991). Drosophila genes *Posterior Sex Combs* and *Suppressor two of zeste* encode proteins with homology to the murine *bmi-1* oncogene. *Nature* **353**, 351-353.

Chisaka, O. and Capecchi, M. R. (1991). Regionally restricted developmental defects resulting from targeted disruption of the mouse homeobox gene *hox-1.5*. *Nature* **350**, 473-479.

Chisaka, O., Musci, T. S. and Capecchi, M. R. (1992). Developmental defects of the ear, cranial nerves and hindbrain resulting from targeted disruption of the mouse homeobox gene *Hox-1.6*. *Nature* **355**, 516-520.

Coré, N., Bel, S., Gaunt, S. J., Aurrand-Lions, M., Pearce, J., Fisher, A. and Djabali, M. (1997). Altered cellular proliferation and mesoderm patterning in Polycomb-M33-deficient mice. *Development* **124**, 721-729.

DeCamillis, M., Cheng, N., Pierre, D. and Brock, H. W. (1992). The *polyhomeotic* gene of *Drosophila* encodes a chromatin protein that shares polytene chromosome-binding sites with *Polycomb*. *Genes Dev*. **6**, 223-232.

Episkopou, V., Maeda, S., Nishiguchi, S., Shimada, K., Gaitanaris, G. A., Gottesman, M. E. and Robertson, E. J. (1993). Disruption of the transthyretin gene results in mice with depressed levels of plasma retinol and thyroid hormone. *Proc. Natl. Acad. Sci. USA* **90**, 2375-2379.

Gendron-Maguire, M., Mallo, M., Zhang, M. and Gridley, T. (1993). *Hoxa-2* mutant mice exhibit homeotic transformation of skeletal elements derived from cranial neural crest. *Cell* **75**, 1317-1331.

Gilbert, S. F. ed. (1994). *Developmental Biology*, 4th ed., Sinauer Associates Inc., Sunderland, Massachusetts.

Goddard, J. M., Rossel, M., Manley, N. R. and Capecchi, M. R. (1996). Mice with targeted disruption of *Hoxb-1* fail to form the motor nucleus of the VIIth nerve. *Development* **122**, 3217-3228.

Haupt, Y., Alexander, W. S., Barri, G., Klinken, S. P. and Adams, J. A. (1991). Novel zinc finger gene implicated as *myc* collaborator by retrovirally accelerated lymphomagenesis in Eμ-*myc* transgenic mice. *Cell* **65**, 753-763.

Hobert, O., Jallal, B. and Ullrich, A. (1996). Interaction of Vav with ENX-1, a putative transcriptional regulator of homeobox gene expression. *Mol. Cell. Biol.* **16**, 3066-3073.

Hogan, B., Beddington, R., Costantini, F. and Lacy, E. eds. (1994). *Manipulating the Mouse Embryo*. Cold Spring Harbor Laboratory Press, New York.

Hunt, P., Gulisano, M., Cook, M., Sham, M.-H., Faiella, A., Wilkinson, D., Boncinelli, E. and Krumlauf, R. (1991a). A distinct *Hox* code for the brachial region of the vertebrate head. *Nature* **353**, 861-864.

Hunt, P., Wilkinson, D. and Krumlauf, R. (1991b). Patterning the vertebrate head: murine Hox 2 genes mark distinct subpopulations of premigratory and migrating cranial neural crest. *Development* **112**, 43-50.

Hunt, P., Whiting, J., Muchamore, I., Marshall, H. and Krumlauf, R. (1991c). Homeobox genes and models for patterning the hindbrain and brachial arches. *Development* **112 Supplement**, 187-196.

Jegalian, B. G. and De Robertis, E. M. (1992). Homeotic transformations in the mouse induced by overexpression of a human *Hox3. 3* transgene. *Cell* **71**, 901-910.

Kaufman, M. H., ed. (1992). *The Atlas of Mouse Development*. Academic Press, San Diego.

Kirby, M. L. and Waldo, K. L. (1990). Role of neural crest in congenital heart disease. *Circulation* **82**, 332-340.

Krumlauf, R. (1994). *Hox* genes in vertebrate development. *Cell* **78**, 191-201.

Lufkin, T., Dierich, A., LeMeur, M., Mark, M. and Chambon, P. (1991). Disruption of the *Hox-1.6* homeobox gene results in defects in a region corresponding to its rostral domain of expression. *Cell* **66**, 1105-1119.

Manley, N. R. and Capecchi, M. R. (1995). The role of *Hoxa-3* in mouse thymus and thyroid development. *Development* **121**, 1989-2003.

McGinnis, W. and Krumlauf, R. (1992). Homeobox genes and axial patterning. *Cell* **68**, 283-302.

McKusick, V. A., ed. (1992). *Mendelian Inheritance in Man*, pp. 1078-1080. Johns Hopkins Univ. Press, Baltimore.

Motaleb, Md. A., Takihara, Y., Nomura, M., Matsuda, Y., Higashinakagawa, T. and Shimada, K. (1996). Structural organization of the *rae28* gene, a putative murine homologue of the *Drosophila polyhomeotic* gene. *J. Biochem.* (*Tokyo*) **120**, 797-802.

Müller, J., Gaunt, S. and Lawrence, P. A. (1995). Function of the Polycomb protein is conserved in mice and flies. *Development* **121**, 2847-2852.

Nomura, M., Takihara, Y. and Shimada, K. (1994). Isolation and characterization of retinoic acid-inducible cDNA clones in F9 cells: One of the early inducible clones encodes a novel protein sharing several highly

homologous regions with a *Drosophila Polyhomeotic* protein. *Differentiation* **57**, 39-50.

Olson, E. N. and Srivastava, D. (1996). Molecular pathways controlling heart development. *Science* **272**, 671-676.

Paro, R. (1995). Propagating memory of transcriptional states. *Trends Genet*. **11**, 295-297.

Payne, R. M., Johnson, M. C., Grant, J. W. and Strauss, A. W. (1995). Toward a molecular understanding of congenital heart disease. *Circulation* **91**, 494-504.

Pearce, J. J. H., Singh, P. B. and Gaunt, S. J. (1992). The mouse has a *polycomb*-like chromobox gene. *Development* **114**, 921-929.

Pollock, R. A., Jay, G. and Bieberich, C. J. (1992). Altering the boundaries of *Hox3.1* expression: evidence for antipodal gene regulation. *Cell* **71**, 911-923.

Rijli, F. M., Mark, M., Lakkaraju, S., Dierich, A., Dollé, P. and Chambon, P. (1993). A homeotic transformation is generated in the rostral branchial region of the head by disruption of *Hoxa*-2, which acts as a selector gene. *Cell* **75**, 1333-1349.

Sambrook, J., Fritsch, E. F. and Maniatis, T. eds. (1989). *Molecular Cloning: A Laboratory Manual*, 2nd ed., Cold Spring Harbor Laboratory Press, New York.

Sasaki, H. and Hogan, B. L. M. (1993). Differential expression of multiple fork head related genes during gastrulation and axial pattern formation in the mouse embryo. *Development* **118**, 47-59.

Schlant, R. C. and Alexander, R. W. eds. (1994). *Hurst's the Heart: Arteries and Veins*, 8th ed., McGraw-Hill Inc., New York.

Schumacher, A., Faust, C. and Magnuson, T. (1996). Positional cloning of a global regulator of anterior-posterior patterning in mice. *Nature* **383**, 250-253.

Shprintzen, R. J., Goldberg, R. B., Lewin, M. L., Sidoti, E. J., Berkman, M. D., Argamaso, R. V. and Young, D. (1978). A new syndrome involving cleft palate, cardiac anomalies, typical faces, and learning disabilities: Velo-cardio-facial syndrome. *Cleft Palate J*. **15**, 56-62.

Simon, J. (1995). Locking in stable states of gene expression: transcriptional control during *Drosophila* development. *Curr. Opin. Cell Biol*. **7**, 376-385.

Studer, M., Lumsden, A., Ariza-McNaughton, L., Bradley, A. and Krumlauf, R. (1996). Altered segmental identity and abnormal migration of motor neurons in mice lacking *Hoxb-1*. *Nature* **384**, 630-634.

Tagawa, M., Sakamoto, T., Shigemoto, K., Matsubara, H., Tamura, Y., Ito, T., Nakamura, I., Okitsu, A., Imai, K. and Taniguchi, M. (1990). Expression of novel DNA-binding protein with zinc finger structure in various tumor cells. *J. Biol. Chem*. **265**: 20021-20026.

Takao, A., Ando, M., Cho, K., Kinouchi, A. and Murakami, Y. (1980). Etiologic categorization of common congenital heart disease. In *Etiology and Morphogenesis of Congenital Heart Disease* (eds. R. Van Praagh and A. Takao), pp. 253-269. Futura, New York.

Takeuchi, T., Yamazaki, Y., Katoh-Fukui, Y., Tsuchiya, R., Kondo, S., Motoyama, J. and Higashinakagawa, T. (1995). Gene trap capture of a novel mouse gene, *jumonji*, required for neural tube formation. *Genes Dev.* **9**, 1211-1222.

van der Lugt, N. M. T., Domen, J., Linders, K., van Roon, M., Robanus-Maandag, E., te Riele, H., van der Valk, M., Deschamps, J., Sofroniew, M., van Lohuizen, M. and Berns, A. (1994). Posterior transformation, neurological abnormalities, and severe hematopoietic defects in mice with a targeted deletion of the *bmi-1* proto-oncogene. *Genes Dev*. **8**, 757-769.

van der Lugt, N. M. T., Alkema, M., Berns, A. and Deschamps, J. (1996). The *Polycomb*-group homolog Bmi-1 is a regulator of murine *Hox* gene expression. *Mech. Dev.* **58**, 153-164.

van Lohuizen, M., Verbeek, S., Scheijen, B., Wientjens, E., van der Gulden, H. and Berns, A. (1991a). Identification of cooperating oncogenes in Eμ-*myc* transgenic mice by provirus tagging. *Cell* **65**, 737-752.

van Lohuizen, M., Frasch, M., Wientjens, E. and Berns, A. (1991b). Sequence similarity between the mammalian *bmi*-1 proto-oncogene and the *Drosophila* regulatory genes *Psc* and *Su(z)2*. *Nature* **353**, 353-355.

Wakamatsu, Y. and Kondoh, H. (1990). Conditions for detection of embryonic N-myc expression by *in situ* hybridization. *Acta Histochem. Cytochem*. **23**, 367-374.

Wilson, D. I., Burn, J., Scambler, P. and Goodship, J. (1993). DiGeorge syndrome: part of CATCH 22. *J. Med. Genet*. **30**, 852-856.

(Accepted 26 June 1997)